WANG, Huilong; WANG, Shengwei. A hierarchical optimal control strategy for continuous demand response of building HVAC systems to provide frequency regulation service to smart power grids. Energy, 2021, 230: 120741.

https://doi.org/10.1016/j.energy.2021.120741

A hierarchical optimal control strategy for continuous demand response of building HVAC systems to provide frequency regulation service to smart power grids

Huilong Wang[1,2] and Shengwei Wang[1,*]

[1] Department of Building Services Engineering, The Hong Kong Polytechnic University, Kowloon, Hong Kong

[2] Research Institute of Sustainable Urban Development, The Hong Kong Polytechnic University, Kowloon, Hong Kong

Abstract: Ensuring the power balance and reliability of power grids is an increasing challenge due to the increasing involvement of intermittent renewable power generations. The use of existing heating, ventilation and air-conditioning (HVAC) systems in buildings has attracted increasing attention to implement continuous demand response in providing frequency regulation service, which can enhance instantaneous power balance and reliability of power grids without extra huge investment. However, the energy flexibility of buildings is not consistent, and the capacity available for frequency regulation service changes over time due to the changes of working conditions. In this study, a hierarchical optimal control strategy, consisting of a regulation bidding controller and a power use following controller, is proposed. It optimizes the power use baseline and regulation capacity, and controls HVAC systems to provide qualified frequency regulation service, considering the tradeoff between financial reward (regulation capacity) and thermal comfort while satisfying the operating constraints of HVAC systems. The proposed control strategy is validated on a simulation test platform. Results show that the strategy can maximize the use of regulation capacity provided by HVAC systems while ensuring the indoor environment control quality under a given guarantee rate.

Keywords: building demand response; optimal control; HVAC systems; grid-responsive building; smart grid.

** Corresponding author: Shengwei Wang, email: beswwang@polyu.edu.hk*

Nomenclature

A	geometric area (m^2)
ACE	area control error
ACH	air changes per hour
AGC	automatic generation control
AHU	air handling unit
C	capacitance (J/K)
C_{air}	specific heat capacity of air (J/kg·K)
C_{reg}	regulation capacity (W)
C_{water}	specific heat capacity of water (J/kg·K)
COP	coefficient of performance
f	conversion coefficient
h	enthalpy (J/kg)
I_{solar}	global solar radiation (W/ m^2)
ICC	International Commerce Centre
i	number of the signal point
MAO	maximum accumulated offset
MTO	maximum temperature offset (°C)
m	flow rate (kg/s)
n_1-n_4, c_1-c_2	coefficients
P	power use (W)
PJM	Pennsylvania-New Jersey Maryland Interconnection, regional transmission organization
PLR	part load ratio
Q	cooling or heating supply/load (W)
R	resistance (K/W)
r	total number of signal points within an hour
s(i)	value of this point
T	temperature (°C)
V	volume of indoor space (m^3)
VFD	variable frequency drive
x	time interval between two continuous signal points

Greek letters

α	air change rate
β	relative efficiency to correct the rated COP under different PLRs
γ	guarantee rate
τ	time constant

Subscripts

b	baseline
c	controller
cf	comfort
chw	chilled water
d	designed
h	high

i	indoor
inf	infiltration
l	low
m	internal mass
ma	manager
n	nominal
neg	negative
o	outdoor
oc	occupant
op	operating
pos	positive
Pre	predicted
r	return
s	steady-state
set	setpoint
sup	supply
w	wall
win	window

1. Introduction

The instantaneous balance and reliability of power grids (reflect in power grid frequency) is conventionally guaranteed through frequency regulation provided at the supply side. However, more frequency regulation capacity will be needed due to the increasing involvement of intermittent renewable power generations [1].

Recently, more policies have been passed to encourage demand resources to provide frequency regulation service (through continuous demand response) with monetary incentives [1, 2]. The process and mechanism for the demand side to provide this service is elaborated as follows. The authorities of power grids calculate the "area control error" (ACE), the magnitude of the power imbalance between the supply side and the demand side. Then, the ACE is transformed and normalized to automatic generation control (AGC) signal (a frequency regulation signal from -1 to 1 for each signal point), and sent to participants involved [3]. The time interval between two continuous signal points is normally from 2 to 4 seconds [4, 5]. To provide this service to power grids, demand resources should implement continuous demand response, i.e., continuously manipulate their power use timely and accurately to follow the AGC signal. Note that demand resources can bid different regulation capacities according to their own flexibility for feasible financial rewards. Even small power consumers are encouraged to provide this service [6]. A large

number of small power consumers can provide a large regulation capacity collectively, and can effectively help power grids to relieve power imbalance. In this way, the frequency of power grids can be maintained within an acceptable range. On the other hand, the authorities of power grids would test whether the power of demand resources can follow the AGC signal properly. For example, an electric power organization, PJM (Pennsylvania-New Jersey Maryland Interconnection, regional transmission organization) uses performance scores to quantify the quality of frequency regulation service provided by the demand side participants [1]. A participant is only qualified when it can get a composite performance score not less than 0.75 [7]. Among various types of demand resources, heating, ventilation and air-conditioning (HVAC) systems in buildings are one of the most promising sources to provide this service [8]. It is because they account for a large proportion of electric energy consumption [9, 10] and have great power use flexibility [11, 12].

Power grids also require the participants to bid their power use baseline (P_b) and regulation capacity (C_{reg}) prior to each bidding time interval [13]. Here, P_b normally refers to the original power use required by demand resources for their main functions. For HVAC systems, P_b normally refers to the power needed for maintaining the indoor temperature. C_{reg} is the capacity provided for frequency regulation service, i.e., the power use modulation magnitude around P_b. Participants prefer to provide regulation capacity as much as possible, which can normally bring more financial rewards [7]. This bidding mechanism in the frequency regulation market is very important, which allows demand resources to provide proper regulation capacities according to their current flexibility without interfering with their main functions. Fabietti et al. [14] and Lymperopoulos et al. [15] proposed a stochastic model-predictive control (MPC) controller to determine the P_b and C_{reg} of an HVAC system, and validated the control method in the electricity market of Switzerland. In the Swiss electricity market, participants are required to provide a P_b schedule and to bid a single C_{reg} for the following week [13]. This rule is not favorable for HVAC systems since the C_{reg} is sometimes quite limited (at night or the peak hour). To provide a constant C_{reg}, the flexibility of building HVAC systems at other times would be wasted. Gorecki et al. [16] proposed a multiple layers control strategy, to determine (one day ahead) the P_b and C_{reg} of an electric heater. Similarly, a three-layer control strategy was developed by Vrettos et al. [17, 18] to bid P_b and C_{reg} one day ahead for fans in HVAC systems. In the study of Cai and Braun [13], a variable-speed rooftop unit (belongs to chillers/heat pumps) was used for providing frequency regulation service. A control

strategy for C_{reg} resetting (once an hour) was developed to maximize C_{reg} considering the operating constraints of the HVAC system, while the constraints associated with thermal comfort (indoor temperature) were neglected. The reason is that in their previous study [19], it was found that providing frequency regulation service did not affect the indoor temperature significantly. Actually, this observation might be reasonable for buildings with small internal heat gain (e.g., residential buildings) as a large proportion power use can be changed with a little impact on thermal comfort (indoor temperature) [20]. However, for buildings with large internal heat gain (e.g., office buildings & commercial buildings), the same proportion power use change can significantly impact the thermal comfort (indoor temperature) [20]. Therefore, under this circumstance, the constraints associated with thermal comfort should also be considered. Especially, this constraint should be more seriously considered when adopting chillers/heat pumps rather than other components to provide this service. The reason is that compared with fans or pumps, chillers/heat pumps consume much more power [21], which technically can provide a larger regulation capacity [22] and have a larger impact on indoor temperature. However, no study can be found in the literature that addresses the optimal control of the P_b and C_{reg} for chillers to provide frequency regulation service, considering both the operating constraints of HVAC systems and the constraints associated with thermal comfort. The tradeoff between financial reward (regulation capacity) and thermal comfort hasn't been considered either.

In this paper, a hierarchical optimal control strategy, consisting of a regulation bidding controller and a power use following controller, is proposed for HVAC systems to provide frequency regulation service to power grids. The main innovations and original contributions of this work include: (1) The online optimal control issue for HVAC systems to provide frequency regulation service is effectively addressed. This strategy can optimize the P_b and C_{reg}, and controls HVAC systems to provide qualified frequency regulation service, considering the tradeoff between financial reward and thermal comfort while satisfying the operating constraints of HVAC systems; (2) A "maximum accumulated offset" (MAO) module in the control strategy is developed by analyzing the relationship between frequency regulation signal and the impact of service on thermal comfort (indoor temperature). This module can help to solve the stochastic optimization problem of bidding regulation capacity in an efficient way. In addition, the positive and negative parts of the MAO module are separately considered, which allows it to work more effectively to maximize the regulation capacity while ensuring the thermal comfort; (3) To modulate the power

of an HVAC system to follow the AGC signal in real time, the chilled water supply temperature setpoint ($T_{chw,supply,set}$) and the indoor temperature setpoint ($T_{i,set}$) are modulated simultaneously, which can guarantee the response speed and response amount of the power use of the HVAC system. This can, therefore, ensure the quality of frequency regulation service. Control tests are conducted on a TRNSYS-MATLAB co-simulation platform to test and validate the proposed control strategy.

2. A hierarchical optimal control strategy

2.1. Outline of the control strategy

Fig. 1 shows the outline of the hierarchical optimal control strategy for HVAC systems to provide the frequency regulation service. This strategy consists of a regulation bidding controller and a power use following controller. The function of the regulation bidding controller is to determine the power use baseline (P_b) and regulation capacity (C_{reg}). The function of the power use following controller is to determine the reference power use according to AGC signal, as the power use setpoint of an HVAC system, and to control the power of the HVAC system to follow this reference power use. In this study, a chiller in cooling mode is used to provide frequency regulation service following the RegA signal (a type of AGC signal with a relatively low frequency). As the power use of fans are affected, it is also considered in this study. In Fig.1, Q_{HVAC} is the cooling supply of HVAC systems. T_i is the current indoor temperature and $T_{i,set,oc}$ is the indoor temperature setpoint determined by occupants.

In this study, the PJM electricity market is used as a reference, where the frequency regulation belongs to an hour-ahead market. This means that the P_b and C_{reg} should and could only be reset once an hour. The regulation bidding controller, therefore, runs once an hour while the power use following controller operates continuously when controlling HVAC systems to provide frequency regulation service.

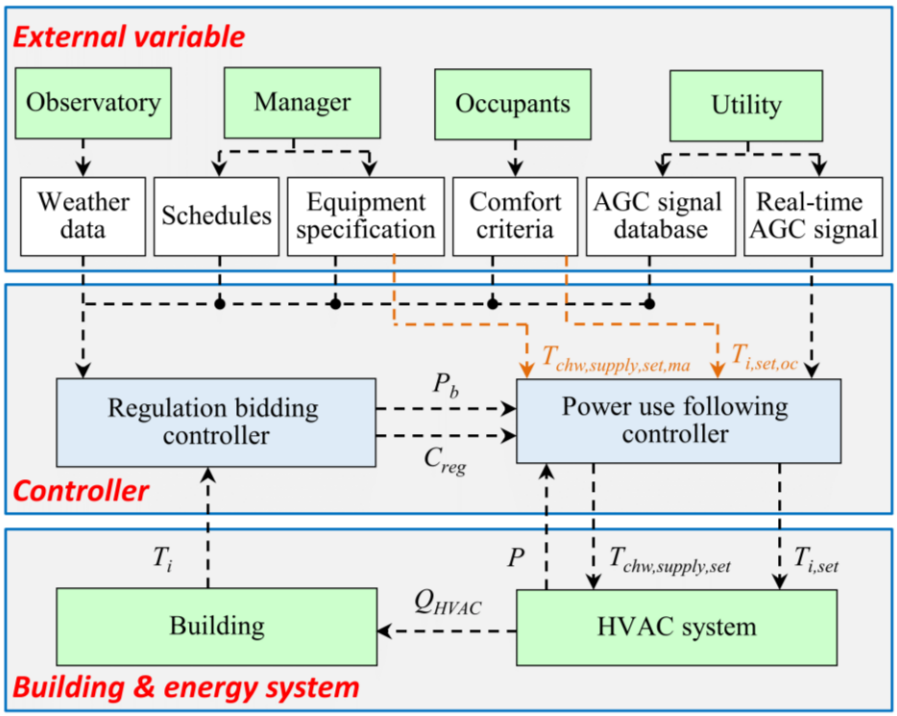

Fig. 1. Outline of the hierarchical optimal control strategy for HVAC systems to provide frequency regulation service.

2.2. Power use following controller

As mentioned in Section 2.1, the function of the power use following controller is to determine the reference power use (P_{set}) and to control the power of the HVAC system to follow this P_{set}. The mechanism of this controller is shown in Fig. 2.

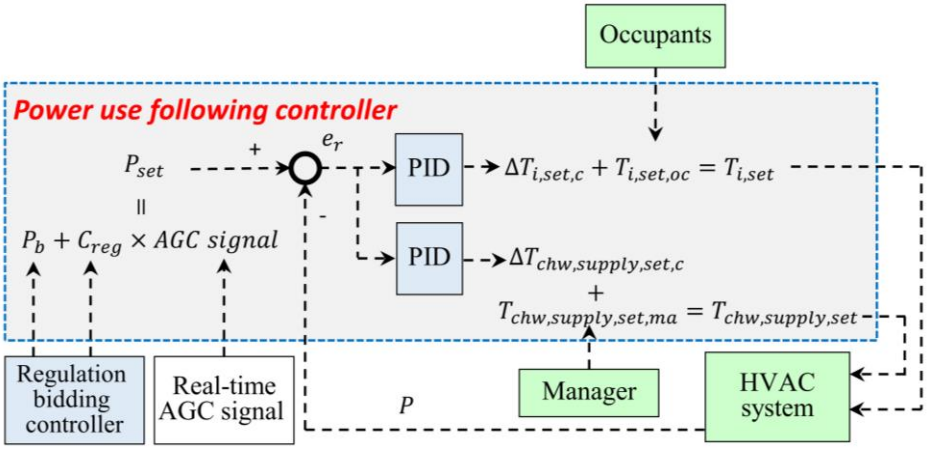

Fig. 2. Mechanism of the power use following controller.

$$P_{set} = P_b + C_{reg} \times AGC\ signal \quad (1)$$

P_{set} is calculated by Eq. (1). Here, AGC signal (i.e., frequency regulation signal) is given by power grids directly. As mentioned in the Introduction, the AGC signal has been normalized to a range from -1 to 1. Therefore, the range of P_{set} is from P_b - C_{reg} to P_b+C_{reg}. In this study, to modulate the power use of the chiller, the indoor temperature setpoint ($T_{i,set}$) and chilled water supply temperature setpoint ($T_{chw,supply,set}$) are changed simultaneously by the power use following controller. As shown in Eqs. (2)-(3), $T_{i,set,oc}$ and $T_{chw,supply,set,ma}$ are determined by occupants and the manager of HVAC systems respectively while $\Delta T_{i,set,c}$ and $\Delta T_{chw,supply,set,c}$ are determined by two proportional integral derivative (PID) sub-controllers included in the power use following controller. In this study, the Ziegler-Nichols (ZN) method [23] is firstly used to initially determine the parameters of the PID controllers. Then a subsequent tuning is conducted manually until the controllers can achieve a satisfied performance. Specifically, the measured power use can follow its setpoint properly and achieve a composite performance score not less than 0.75, as mentioned in the Introduction.

$$T_{i,set} = T_{i,set,oc} + \Delta T_{i,set,c} \tag{2}$$

$$T_{chw,supply,set} = T_{chw,supply,set,ma} + \Delta T_{chw,supply,set,c} \tag{3}$$

Modulating $T_{chw,supply,set}$ can directly affect the power use of chillers, which can guarantee the response speed of the power use. However, it is found in our preliminary tests that some issues could be caused when the regulation capacity is large. For example, when the AGC signal point changes, the power use of HVAC systems is required to change. However, the cooling demand would not change if the indoor temperature setpoint is unchanged. The change of power use and the unchanged cooling demand conflict with each other. When a small regulation capacity is provided, this conflict is not that significant due to the buffer of the thermal inertia of buildings and HVAC systems. However, when the regulation capacity is large and a great response amount of the power use is required, this conflict could result in a failure that the power use cannot follow P_{set}. As a result, in this study, $T_{i,set}$ and $T_{chw,supply,set}$ are changed simultaneously, which can guarantee both the response speed and response amount of the power use of HVAC systems.

2.3. Description of models used in the regulation bidding controller

To establish the regulation bidding controller, two models are needed, including a building thermodynamic model and an HVAC system power use model.

2.3.1. Building thermodynamic model

The building thermodynamic model used in the controller should consider both computational efficiency and accuracy. It should adequately capture the thermal behaviors of buildings to ensure its robustness under different conditions. To meet these requirements, a grey-box thermal model is finally developed. The development and validation of this model can be found in Appendix A and Appendix B, respectively. More details about the construction of a grey-box thermal model could be found in our previous work [24].

2.3.2. HVAC power use model

The predicted power use of chillers $P_{chiller,pre}$ can be determined according to the predicted cooling supply $Q_{HVAC,pre}$ and *COP* (coefficient of performance), as shown in Eq. (4). The COP under different cooling supply is obtained according to the chiller model under steady state, as shown in Eq. (C.3) and Eq. (C.4) in Appendix C.

$$P_{chiller,pre} = \frac{Q_{HVAC,pre}}{COP} \tag{4}$$

As mentioned above, although chillers are mainly used to provide frequency regulation service in this study, the power use variation of fans is also considered. The predicted power use of fans $P_{fan,pre}$ can be determined according to Eqs. (5)-(8). Here, Eq. (5) is a designed case when the fan is under rated power use, with subscript of *d*, while Eq. (6) represents any case in operation. Where *Q* is the cooling supply. m_{air} is the air flow rate. h_r and h_{sup} are enthalpy value of return air and supply air, respectively. In prediction, the enthalpy value of return air $h_{r,pre}$ and supply air $h_{sup,pre}$ in the following hour can be directly assumed the same as that in current hour. Final, according to the affinity law [25], the power use of fans can be predicted, as shown in Eq. (8).

$$Q_d = m_{air,d}(h_{r,d} - h_{sup,d}) \tag{5}$$

$$Q_{HVAC,pre} = m_{air,pre}(h_{r,pre} - h_{sup,pre}) \tag{6}$$

$$\frac{m_{air,pre}}{m_{air,d}} = \frac{Q_{HVAC,pre}}{Q_d} \times \frac{h_{r,d} - h_{sup,d}}{h_{r,pre} - h_{sup,pre}} \tag{7}$$

$$P_{fan,pre} = P_{fan,rated}\left(\frac{m_{air,pre}}{m_{air,d}}\right)^3 \tag{8}$$

2.4. Regulation bidding controller

2.4.1. Mechanism of the regulation bidding controller

As mentioned in Section 2.1, the function of the regulation bidding controller is to determine the P_b and C_{reg}. The mechanism of this controller is shown in Fig. 3.

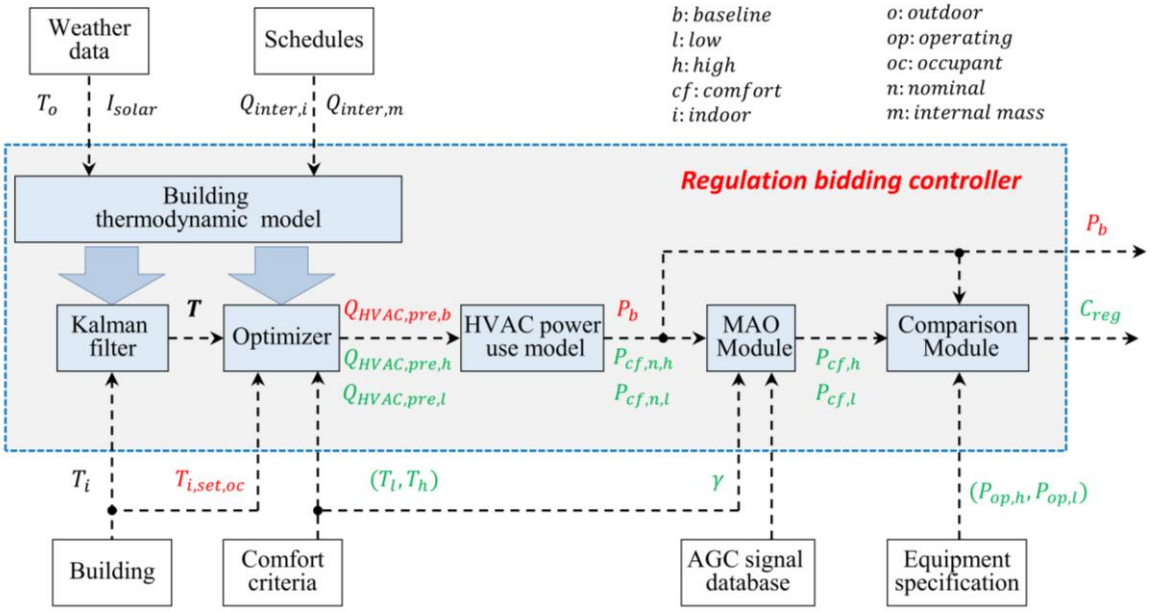

Fig. 3. Mechanism of the regulation bidding controller.

2.4.2. Power use baseline

As mentioned in the Introduction, the P_b refers to the power use needed to maintain the indoor temperature setpoint $T_{i,set,oc}$. In this study, P_b is obtained in three steps.

<u>*Step One*</u> – Obtain the current state of the building. In our case, the state includes four variables: $\boldsymbol{T} = (T_{w,o}\ T_{w,i}\ T_i\ T_m)$, the temperature of the out wall, interior wall, indoor air and internal mass, respectively (details are present in Appendix A). However, only T_i could be measured in practice. To address this issue, a Kalman filter is used to estimate the other immeasurable variables [26].

<u>*Step Two*</u> - An optimizer is used to predict the cooling demand $Q_{HVAC,pre,b}$ to maintain the indoor temperature setpoint $T_{i,set,oc}$ according to the current state variables $\boldsymbol{T}$ of the building, the weather data (T_o: outdoor air temperature and I_{solar}: global solar radiation), and the internal heat gains ($Q_{inter,i}$: internal heat gain to indoor air and $Q_{inter,m}$: internal heat gain to internal thermal mass). These internal heat gains are obtained based on the schedules of occupants, lighting, and

equipment. There are many studies conducted for the prediction of weather data and the schedules which are not the focus of this work. Therefore, these variables in the following hour are assumed known in advance. The optimization problem is shown in Eqs. (9)-(10). Here, the $T_{i,pre}$ is the predicted indoor temperature at the end of the following hour. The discretization time of the building thermodynamic model in Eq.(10-b) is three minutes after considering the balance between the operation speed and prediction accuracy.

$$\min_{Q_{HVAC,pre,b}} \left| T_{i,pre} - T_{i,set,oc} \right| \tag{9}$$

Subject to

$$0 \le Q_{HVAC,pre,b} \le Q_{HVAC,rated} \tag{10-a}$$

$$T_{i,pre} = Building\ model(\boldsymbol{T}, T_o, I_{solar}, Q_{inter,i}, Q_{inter,m}, Q_{HVAC,pre,b}) \tag{10-b}$$

The building thermodynamic model is a linear state space model and the relationship between $Q_{HVAC,pre,b}$ and $T_{i,pre}$ is monotonic. Therefore, this optimization problem could be effectively solved.

<u>*Step Three*</u> - The HVAC system power use model is adopted to predict the corresponding power use baseline P_b.

$$P_b = P_{chiller,pre} + P_{fan,pre} \tag{11}$$

2.4.3. Regulation capacity

Participants prefer to provide regulation capacity as much as possible, which can normally bring more financial rewards. However, there are two types of constraints. The first type is the operating constraints of HVAC systems ($P_{op,h}$ and $P_{op,l}$). Here, subscript *h* and *l* represent high and low, respectively. Another type is the constraints associated with the thermal comfort of occupants ($P_{cf,h}$ and $P_{cf,l}$). With these constraints and the power use baseline P_b, the regulation capacity C_{reg} can be determined by the comparison module (in Fig. 3). Note that C_{reg} cannot be negative.

$$C_{reg} = min(P_{op,h} - P_b, P_{cf,h} - P_b, P_b - P_{op,l}, P_b - P_{cf,l}) \tag{12}$$

The following parts present the process to obtain these constraints.

Operating constraints: Operating constraints are inherent limitations for HVAC systems to provide frequency regulation service. In this study, the operating constraints of the HVAC system $P_{op,h}$ is defined as the total power of chillers and fans corresponds to $Q_{HVAC,rated}$, namely $P_{chiller,rated}$

added by $P_{fan,rated}$ and $P_{op,l}$ is defined as the total power of chillers and fans corresponds to $10\% \cdot Q_{chiller,rated}$. The reason is as follows. For centrifugal chillers, there are three distinct operation mechanisms to change power use, which are originally designed for capacity control, including variable frequency drive (VFD), inlet vane control, and hot gas bypass. A VFD is normally used to reduce the cooling supply of a chiller from its rated capacity by decreasing the compressor speed, typically to about 60% of the rated speed [27]. To further reduce the cooling supply, the inlet vane is used to decrease the refrigerant volume flow rate through the centrifugal compressor [28]. At the lowest capacity level, normally 10% of rated capacity [29], the hot gas bypass is used to change the cooling output. This is inefficient because it has a quite limited impact on power use and should be avoided when providing frequency regulation service [4].

Comfort constraints: Another type of constraints is associated with the thermal comfort of occupants ($P_{cf,h}$ and $P_{cf,l}$). According to Eq. (1) in Section 2.2, it can be found that the power use of HVAC systems deviates from their power use baselines when providing frequency regulation service. This would naturally affect the cooling/heating supply of HVAC systems, which eventually affect indoor temperature. Therefore, the comfort criteria (i.e., indoor temperature range) set by occupants can also constrain HVAC systems to provide frequency regulation service. Actually, since the AGC signal is unpredictable [14], the impact of providing frequency regulation service on indoor environment control is also unpredictable. Therefore, it is a stochastic optimization problem to determine the constraints. In this study, a "maximum accumulated offset" (MAO) module is developed, which can solve this problem in an efficient way. This module is developed based on two prerequisites. The prerequisites are introduced in Section 2.4.4, and the steps to determine comfort constraints are introduced in Section 2.4.5.

2.4.4. Prerequisites for the method to determine the comfort constraints

<u>*Prerequisite One*</u> - The hourly "maximum accumulated offset" (MAO) of the frequency regulation signal is corresponding to the "maximum temperature offset" (MTO) of the indoor space.

As mentioned in Section 2.1, the demand resources should bid the P_b and C_{reg} at the beginning of each hour in the PJM market. This, on the other hand, also means that buildings have the opportunity to adjust P_b to eliminate the indoor temperature offset caused in the previous hour.

Consequently, the problem of indoor temperature offset due to the manipulation of power use within a given hour would mainly last within this hour.

As mentioned in the Introduction, P_b is the power use needed to maintain the indoor temperature setpoint. Therefore, taking cooling for example, a positive signal point mainly causes a negative offset of indoor temperature, while a negative signal point mainly causes a positive offset of indoor temperature. Consequently, the positive (negative) hourly "maximum accumulated offset" (MAO) of the AGC signal, in principle, would most likely result in the negative (positive) "maximum temperature offset" (MTO) of indoor spaces within an hour (i.e., Prerequisite One).

The hourly MAO of the AGC signals can be calculated by Eqs. (13)-(14), where r is the total number of signal points within an hour (r=1800 in PJM [7]). x is the time interval between two continuous signal points (2 seconds in PJM [7]). i is the number of the signal point while $s(i)$ is the value of this point. As each point of the AGC signal is between -1 and 1, the range of hourly MAO of AGC signal is between $-rx$ and rx (i.e., -3600 to 3600). Particularly, "MAO = rx" means within this hour, the power use setpoint is set as P_b+C_{reg} (according to Eq. (1)) continuously, which most likely causes the maximum indoor temperature decrease (under cooling mode).

$$\max_n \left|\sum_{i=1}^{n} s(i)\right| \quad \{n \in \mathbb{Z} | 1 \le n \le r\} \tag{13}$$

$$MAO = x \cdot \sum_{i=1}^{n} s(i) \tag{14}$$

Take a historical RegA signal for example, as shown in Fig. 4. According to Eq. (13), the maximum accumulated offset point could be found at n = 1560, corresponding to the time point at the 3120th second, as marked as time 'A' in the figure. The MAO of this signal is -1905.34, which is obtained using Eq. (14). This value is actually the area above zero minus the area below zero before time 'A'.

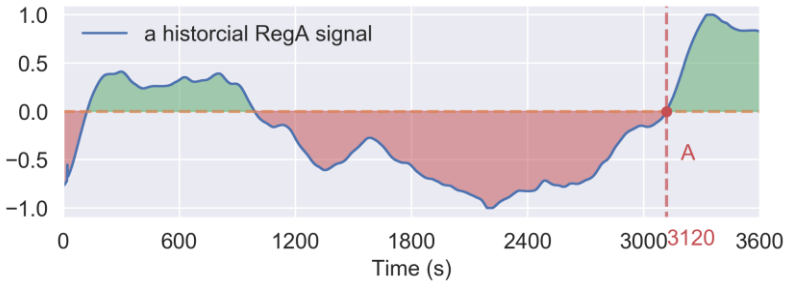

Fig. 4. Calculation of the MAO of a historical RegA signal.

To verify the relationship between the hourly MAO of the AGC signal and the MTO of indoor spaces within an hour, preliminary tests are conducted on a simulation test platform [30] (detailed described in Section 3). The chiller is first controlled to work stably under the conventional control strategy, and then it is controlled to follow an hourly AGC signal. The MTO of the indoor space within this hour and the hourly MAO of the AGC signal are recorded. Tests are conducted by following historical hourly RegA signals in the whole year of 2018, which means that as many as 8,760 cases are conducted. The results are shown in Fig. 5. A small number of cases represented by yellow dots are not typical, which may result from the mismatch between reference power use (P_{set}) and measured power use, or the nonlinear mapping between cooling supply and power use. For most cases (represented by red and blue dots), a larger MAO of the signal can cause a larger MTO of the indoor space with opposite signs. This observation further verifies Prerequisite One.

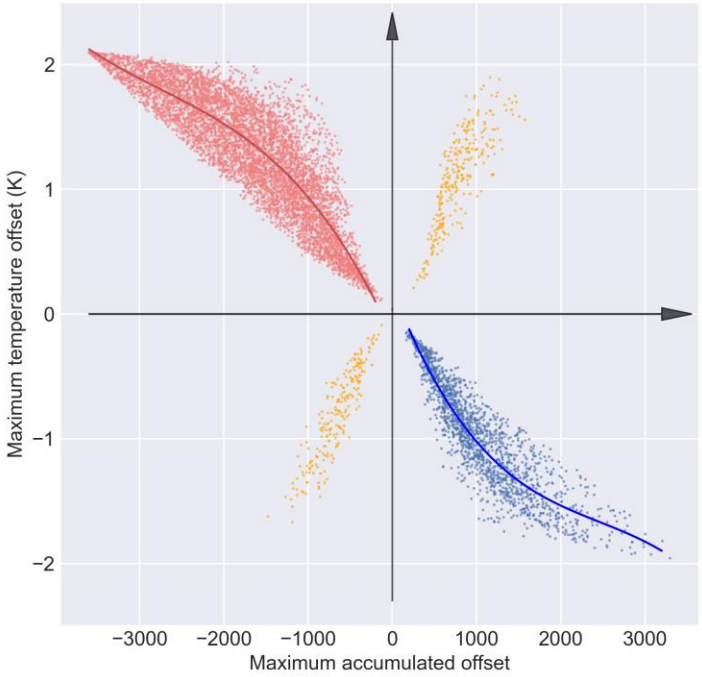

Fig. 5. The hourly maximum accumulated offset of RegA signal and hourly maximum temperature offset of the indoor space when providing frequency regulation service.

Prerequisite Two - Although the AGC signal is unpredictable, the hourly MAO of the AGC signal conforms to a stable probability distribution.

Fig. 6 shows the probability distributions of the hourly MAO of RegA signal in each month in 2018. It proves that the hourly MAO of the AGC signal conforms to a stable probability

distribution. The dashed lines separate the probability distributions into positive parts and negative parts. It can be found that the negative parts are much larger than the positive parts.

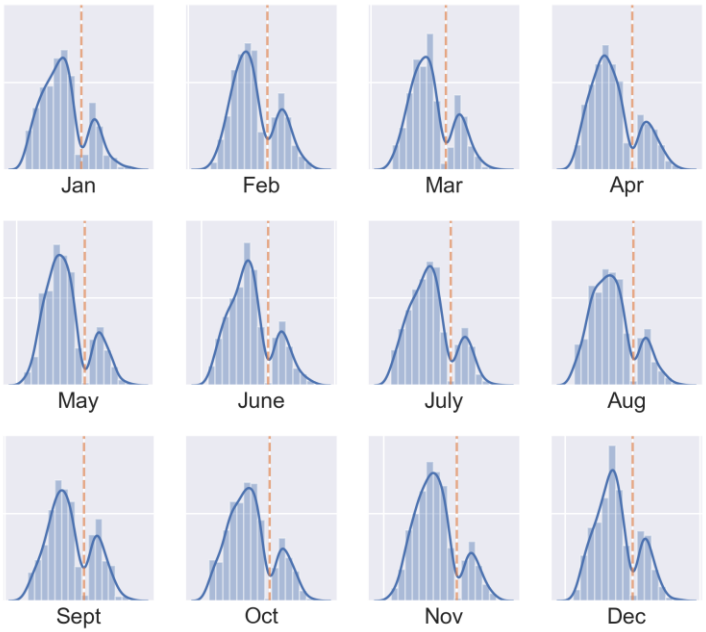

Fig. 6. The probability distribution of hourly maximum accumulated offset of RegA signal in each month in 2018.

2.4.5. Method and steps to determine comfort constraints

Based on the above prerequisites, the constraints associated with thermal comfort ($P_{cf,h}$ and $P_{cf,l}$) can be determined in two steps.

Step One - Consider the worst case when the hourly MAO of AGC signal equals lower limit (-3600) and upper limit (3600) respectively to determine the nominal constraints associated with the thermal comfort ($P_{cf,n,h}$ and $P_{cf,n,l}$). This process is similar to that of calculating the power use baseline P_b. Differently, the $T_{i,set,oc}$ in Eq. (9) is replaced by the allowed indoor temperature limit T_l and T_h, to obtain corresponding $Q_{HVAC,pre,h}$ and $Q_{HVAC,pre,l}$ instead of $Q_{HVAC,pre,b}$ (shown in Fig. 3). Then, the HVAC system power use model is adopted to predict the corresponding $P_{cf,n,h}$ and $P_{cf,n,l}$, respectively.

Step Two - A "maximum accumulated offset" (MAO) module is developed to determine the constraints associated with the thermal comfort ($P_{cf,h}$ and $P_{cf,l}$) considering the tradeoff between financial reward and thermal comfort.

Considering the worst case might ensure that the indoor temperature can be maintained in the comfort range. However, it is also feasible to enlarge the financial reward (regulation capacity) with a little sacrifice of the thermal comfort (i.e., maintaining the indoor temperature within the comfort range with a certain guarantee rate, γ). Fig. 7 shows the positive part and negative part of the cumulative probability distribution of the hourly MAO of the RegA signal in 2018. The positive and negative parts are separately considered, as their distributions are obviously different. In this way, the MAO module can work more effectively to maximize regulation capacity and ensure thermal comfort. In Fig. 7, point *A* means that 90% (γ = 0.9) of the RegA signal that has a positive MAO smaller than 1742 (i.e., $MAO_{pos,0.9} = 1742$). Point *B* means that 90% of the RegA signal that has a negative MAO larger than -2777 (i.e., $MAO_{neg,0.9} = -2777$).

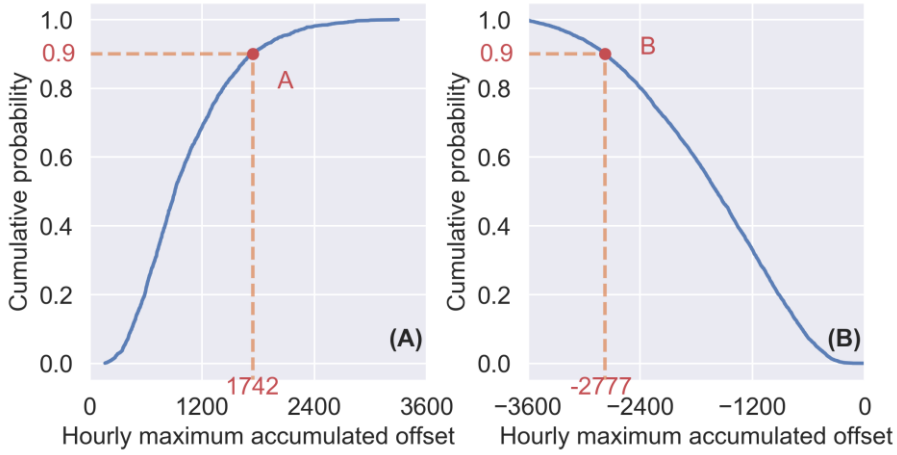

Fig. 7. Cumulative probability distribution of hourly maximum accumulated offset of the RegA signal in 2018 (A) positive (B) negative.

According to the relationship between the hourly MAO of the AGC signal and the MTO of the indoor space shown in "Prerequisite One", the constraints associated with thermal comfort ($P_{cf,h,}$ and $P_{cf,l}$) under a certain guarantee rate can be obtained by Eqs. (15)-(16). In this study, the tradeoff between financial reward and thermal comfort is reflected in γ. A smaller guarantee rate means more sacrifice of thermal comfort and greater financial reward. A larger guarantee rate means less sacrifice of thermal comfort and less financial reward. For example, it is easy to find that if a smaller guarantee rate γ is selected, $P_{cf,h,}$ would increase while $P_{cf,l}$ would decrease. As a result, the regulation capacity provided would finally increase which means a larger financial

reward. In application, managers can determine the minimum guarantee rate to get the maximum financial rewards.

$$\frac{MAO_{pos,\gamma}}{MAO_{pos,100\%}} = \frac{P_{cf,n,h} - P_b}{P_{cf,h} - P_b} \tag{15}$$

$$\frac{MAO_{neg,\gamma}}{MAO_{neg,100\%}} = \frac{P_b - P_{cf,n,l}}{P_b - P_{cf,l}} \tag{16}$$

After all the constraints are obtained, the regulation capacity C_{reg} can be obtained by Eq. (12) mentioned above.

3. Test platform and test arrangement

In the study, a TRNSYS-MATLAB co-simulation test platform is built, as shown in Fig. 8. The regulation bidding controller is built in MATLAB 2014a (32-bit) [31], while the power use following controller and other models (i.e., the building model and the HVAC system models) are built in TRNSYS 18 (32-bit) [32]. The simulation interval in this study is one second.

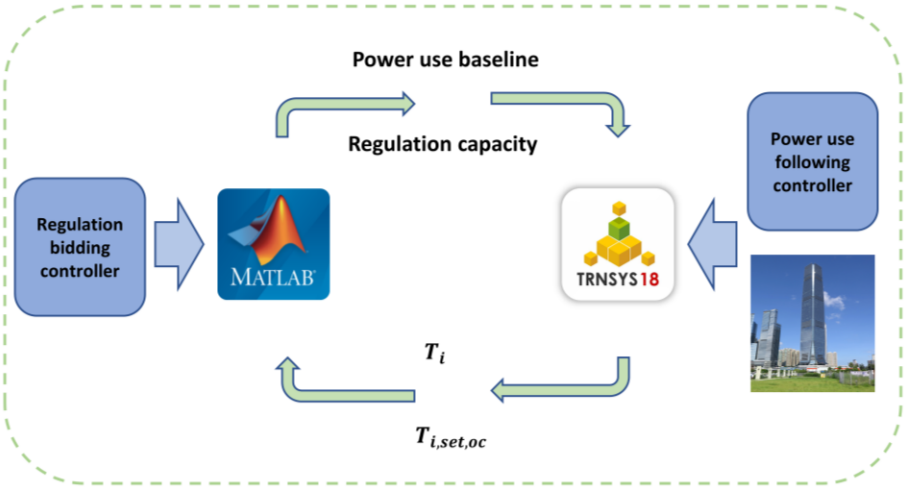

Fig. 8. TRNSYS-MATLAB co-simulation test platform.

The test platform is constructed based on the International Commerce Centre (ICC) in Hong Kong. The building is about 490 m high with a total floor area of approximately 321,000 m^2 served by a typical HVAC system including six identical chillers. The rated cooling capacity and power use of each chiller are 7230 kW and 1270 kW, respectively [33]. In this study, only one chiller, corresponding to hypothetical one-sixth of the total area, is used for providing frequency regulation service. The corresponding total rated power use of fans is 615 kW. In the test platform, only one

floor is built in the TRNSYS for simplification. The models of the building and the HVAC system are introduced as follows.

3.1 Dynamic model of building

In this study, model Type 56 in TRNSYS is used. It is a detailed physical model that can precisely describe the dynamic thermal behavior of a building. The settings in the building model are presented as follows.

Envelope: External walls (10 mm gypsum plaster, 100 mm concrete 10 mm cement/sand render, 5 mm mosaic tiles, and light color semi-glossy paint [34]) and windows (6 mm single-glass) [35].

Internal mass: 100 kg/m^2 wood/plastic material (density: 800 kg/m^3, thermal conductivity: 0.2 w/m·k, specific heat capacity: 1400 J/kg·k, thickness: 0.018 m) [36].

Fresh air and infiltration*:* The building is supplied with fixed amounts of fresh air of 10 L/s per person. The building is relatively tight, thus the infiltration rate is set as 0.1 ACH (air changes per hour) [37].

Internal heat gain: The design density of occupants is 9 m^2 per person. The design lighting power is 30 W/m^2. The design equipment power is 30 W/m^2. The normal patterns of occupant, lighting, and equipment load are shown in Fig. 9. They are expressed in fractions of their respective peak values. The internal gain from occupants, lighting, and equipment can be split into convective and radiative components (occupants heat gains: 40% latent heat, 20% convective and 40% radiative; lighting heat gains: 50% convective and 50% radiative; equipment heat gains: 67% convective and 33% radiative) [37].

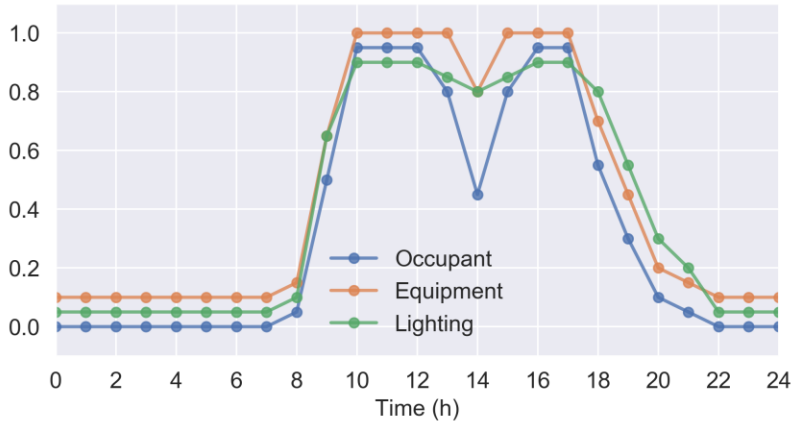

Fig. 9. Normal patterns of occupant load, equipment load, and lighting load.

3.2 Dynamic models of the HVAC system

Different from typical conventional demand response which is used to shift peak load [38-40], frequency regulation service is in a very short timescale (i.e., seconds) [9]. Therefore, using steady-state models could more or less misrepresent the dynamic process of providing frequency regulation service [19]. In this study, dynamic models of the HVAC systems are used.

***Chiller*:** The chiller model is developed by introducing a time constant to the outputs of steady-state models. Details can be found in Appendix C.

***Pump and fan*:** In this study, the power uses of pumps are neglected for simplicity. The reason is that compared pumps, chillers/heat pumps and fans consume much more power [21]. This is also a common simplification when using chillers for providing frequency regulation service [4, 5, 8]. For fans, model Type 147 in TRNSYS is used which can describe the power use of variable speed fans.

Air handling unit (AHU): The steady-state characteristics of AHUs are described by Type 124 in TRNSYS. According to experimental studies on AHUs [41-43], the transient behaviors of an AHU can be described by first-order transfer functions. Therefore, similar to chillers, the dynamic behavior of AHUs can be obtained by introducing a time constant (set as 12 seconds in this study) to the outputs of its steady-state model.

Water and air pipeline: The dynamic behaviors of air flow and water flow are mainly affected by the frequency change of the input power (for variable-speed pumps and fans). According to our previous experimental study [44], after a step change of the frequency of the pump, it only takes 2

seconds for the water flow to return to a new steady-state condition. Thus, a moving average method [45] is used to represent the dynamic behaviors of water flow and air flow. Here, it is assumed that the water pipeline and air pipeline have similar dynamic behaviors. The travel time of the water in the water loop and the travel time of air in the air loop is also considered, as they could have impacts on the response time of chiller power use. These times are estimated based on the practical information of the ICC building.

3.3 Test arrangement

One day is selected to test and validate the control strategy, while only the period from 7:00 to 23:00 is presented in Figs. 10-17. The indoor temperature setpoint determined by occupants ($T_{i,set,oc}$) is 24 °C throughout the day. The comfort range of indoor temperature is from 22°C (T_l) to 26°C (T_h). The guarantee rate for maintaining the indoor temperature within the comfort range is 0.9 (γ). Four cases are conducted and compared in order to test the control performance of the proposed control strategy.

Case 1: The system is operated under conventional control.

Case 2: The system is operated under the proposed control strategy following a hypothetical frequency regulation signal which is constant zero. The aim of this case is to generate a fundamental scenario for comparison.

Case 3: The system is operated under the proposed control strategy following a RegA signal with relatively small hourly maximum accumulated offsets (MAOs).

Case 4: The system is operated under the proposed control strategy following a RegA signal with relatively large hourly MAOs.

Note that for Case 2, Case 3 and Case 4, the system is only under the proposed control strategy from 8:00 to 22:00, while at other times, the system is under conventional control. The indoor temperature setpoint shown in Figs. 10,11,13,16 is the setpoint determined by occupants ($T_{i,set,oc}$) rather than $T_{i,set}$ calculated in Eq. (2).

4. Results and analysis

4.1 Test Case 1: Under conventional control strategy

Fig. 10 shows the measured power use of HVAC systems (i.e., a chiller and fans), indoor temperature (T_i) and its setpoint ($T_{i,set,oc}$) under conventional control strategy. It can be observed that the conventional strategy can effectively control the indoor temperature within the comfort range. The conventional strategy belongs to typical feedback control. Therefore, there is some delay for the HVAC system to change the cooling supply. For example, at 8:00 and 9:00 when there was a rapid increase in cooling load, the room temperature deviated slightly from its setpoint.

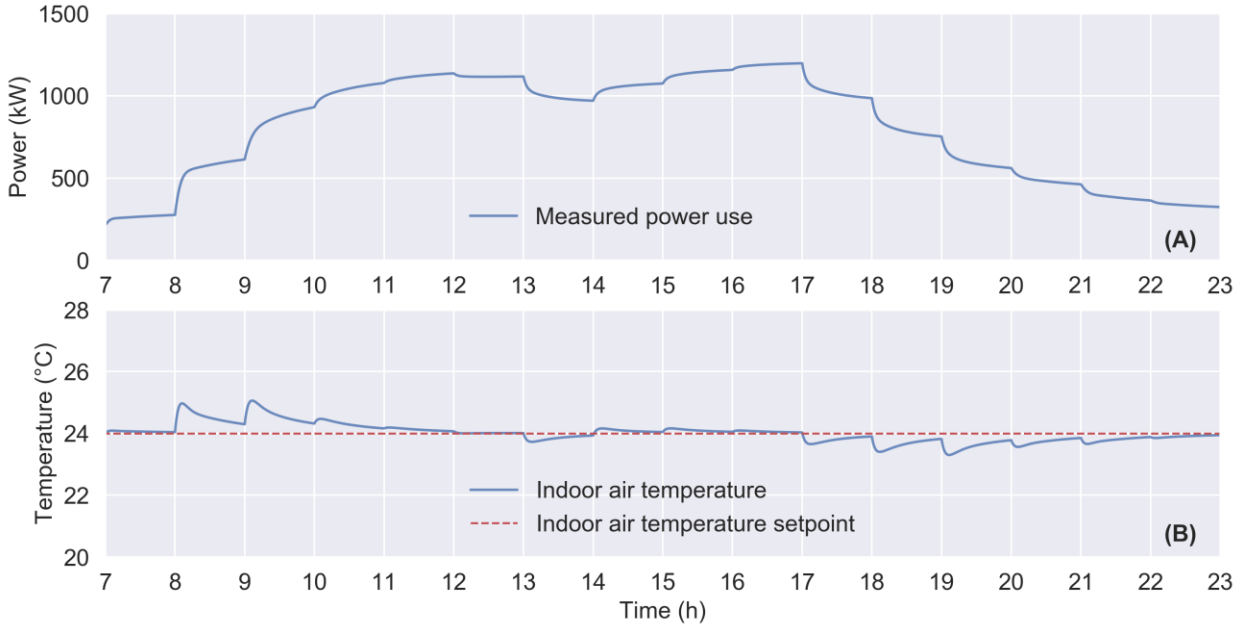

Fig. 10. (A) Power use of the chiller (B) indoor temperature and its setpoint - Test Case 1.

4.2 Test Case 2: Under the proposed control strategy following a constant-zero signal

In this case, a hypothetical constant zero frequency regulation signal is followed. According to Eq. (1) in Section 2.2, it means that the power use baseline (P_b) is directly used as reference power use (P_{set}). The power use of the chiller obtained in this case would be used for comparison with that in Case 3. As observed in Fig. 11, the measured power use can follow the power use baseline properly. As the building thermodynamic model in the controller could precisely predict the cooling demand, the indoor temperature is controlled properly near its setpoint.

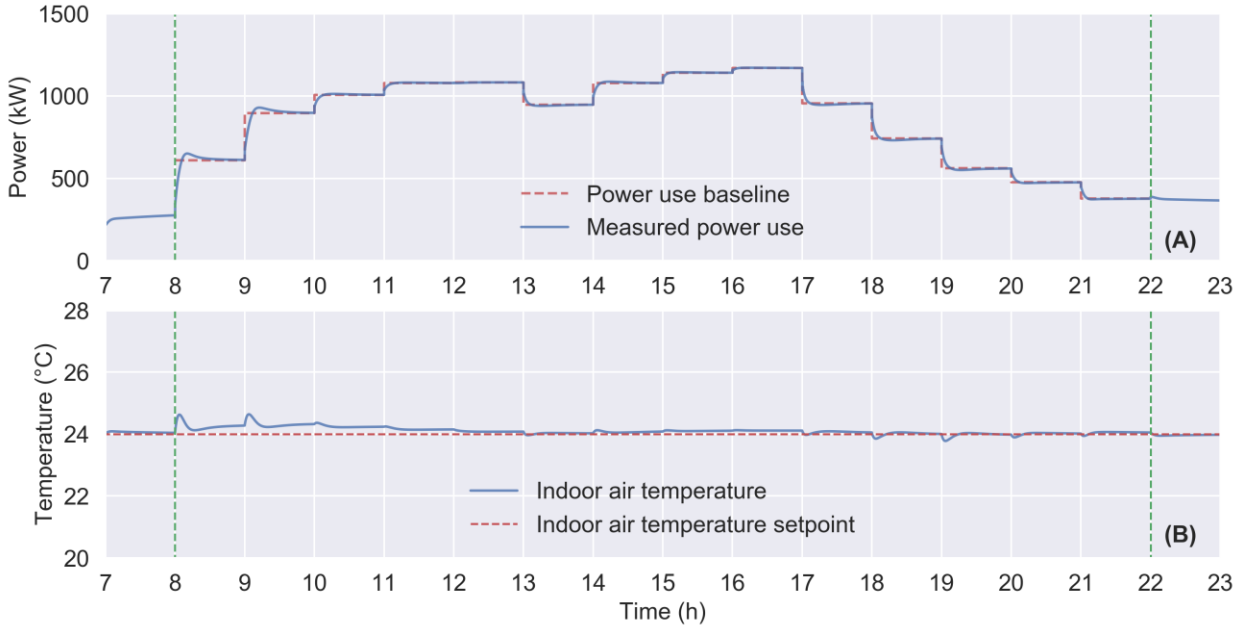

Fig. 11. (A) Power use of the chiller (B) indoor temperature and its setpoint - Test Case 2.

4.3 Test Case 3: Under the proposed control strategy following signal with relatively small hourly maximum accumulated offsets

In Case 3, the system is operated under the proposed control strategy from 8:00 to 22:00 following a historical RegA signal (359th day in 2018) with relatively small absolute hourly MAOs. Fig. 12 shows the P_b and the constraints ($P_{cf,h}$, $P_{cf,l}$, $P_{op,h}$, and $P_{op,l}$) of regulation capacity in each hour. In addition, the P_b in Case 2 is also presented for comparison. Fig. 13 presents the indoor temperature and its setpoint.

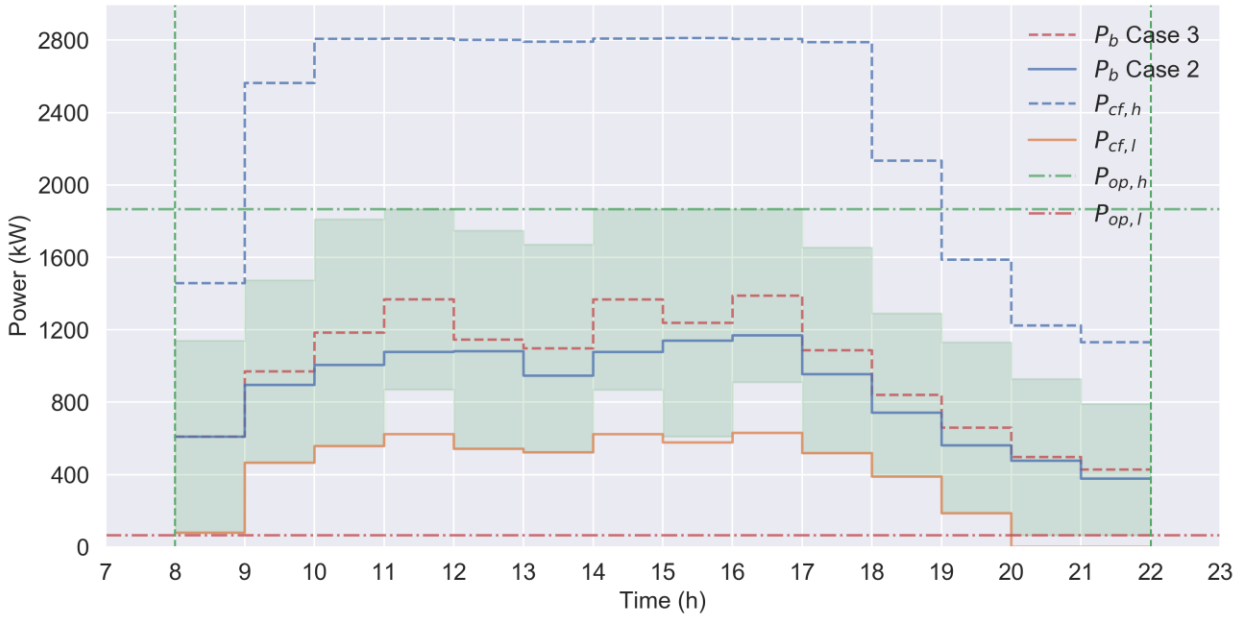

Fig. 12. The power use baseline in Case 2 and the power use baseline and constraints of regulation capacity in Case 3.

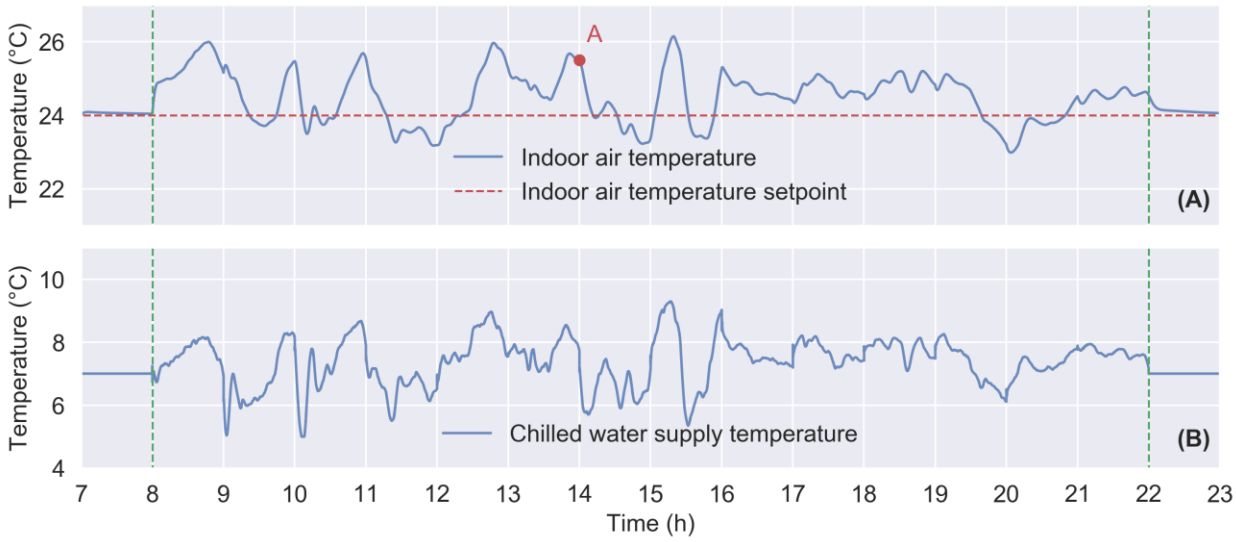

Fig. 13. (A) Indoor temperature and its setpoint (B) chilled water supply temperature - Test Case 3.

It can be found in Fig. 12 that the power use baselines in Case 2 and Case 3 are obviously different. This is because that the proposed control strategy can optimize the power use baseline to maintain the indoor temperature considering both the current state of the building HVAC system and the predicted cooling demand in the following hour. For example, at 14:00, the indoor temperature rose to a value relatively far from its setpoint (point *A* shown in Fig. 13). Therefore,

the regulation bidding controller bid a higher power use baseline in the following hour. As observed in Fig. 12, the power use baseline in Case 3 is significantly larger than that in Case 2 from 14:00 to 15:00.

From Fig. 12, it can also be observed that the difference between $P_{cf,h}$ and the power use baseline P_b is much larger than the difference between the $P_{cf,l}$ and the power use baseline P_b. It is caused by the probability distribution of the hourly MAO of the RegA signal (Fig. 6). As mentioned in Section 2.4.4, the positive part of this probability distribution is much smaller than the negative part. Therefore, the ratio of $MAO_{pos,0.9}$ to $MAO_{pos,100\%}$ (0.48) is smaller than the ratio of $MAO_{neg,0.9}$ to $MAO_{neg,100\%}$ (0.77). Technically, according to Eqs. (15)-(16), a larger regulation capacity normally could be bid for down-reserve (an increase of power use [17]) than that for up-reserve (a decrease of power use [17]). It is allowable in some power grid organizations to bid different capacities for down-reserve and up-reserve [46], while in PJM, the capacities for down-reserve and up-reserve are normally required to be the same. The green area in Fig.12 indicates the final power use range (P_b - C_{reg} to P_b+C_{reg}) when providing frequency regulation service. As observed in Fig. 13, the proposed control strategy can work effectively to maintain the indoor temperature within the comfort range (22°C to 26°C) while bidding a regulation capacity as much as possible, even though the AGC signal is unknown at the time of bidding. As mentioned in Section 2.2, the chilled water supply temperature is controlled to adjust the power use of the system. It can be observed from Fig.13 that the chilled water supply temperature shows a similar trend to the indoor temperature. Differently, it fluctuates more significantly than the indoor temperature, for example, at 9:00 am. It is reasonable as the fluctuation of chilled water supply temperature is compensated by the thermal inertia of indoor air and internal mass.

Fig. 14 presents the power use baseline, reference power use P_{set}, and measured power use in Case 3. Similar to this case, the AGC signal through the year of 2018 (i.e., 365 days) is used, and the quality of the frequency regulation service over the year is assessed using performance scores [7]. The average composite score obtained was 0.792 (correlation score: 0.853, delay score: 0.832, precision score: 0.691). This composite score is higher than 0.75, indicating that the chiller can fulfill the requirements of PJM to provide this service. More investigation on the performance of chillers for providing frequency regulation service can be found in these studies [4, 5, 19].

As mentioned above, at 14:00, the indoor temperature rose relatively far from its setpoint (shown in Fig. 13). The reason can be found in Fig.14. From 13:00 to 14:00, the measured power was significantly lower than the power use baseline, which resulted in a significant increase in the indoor temperature.

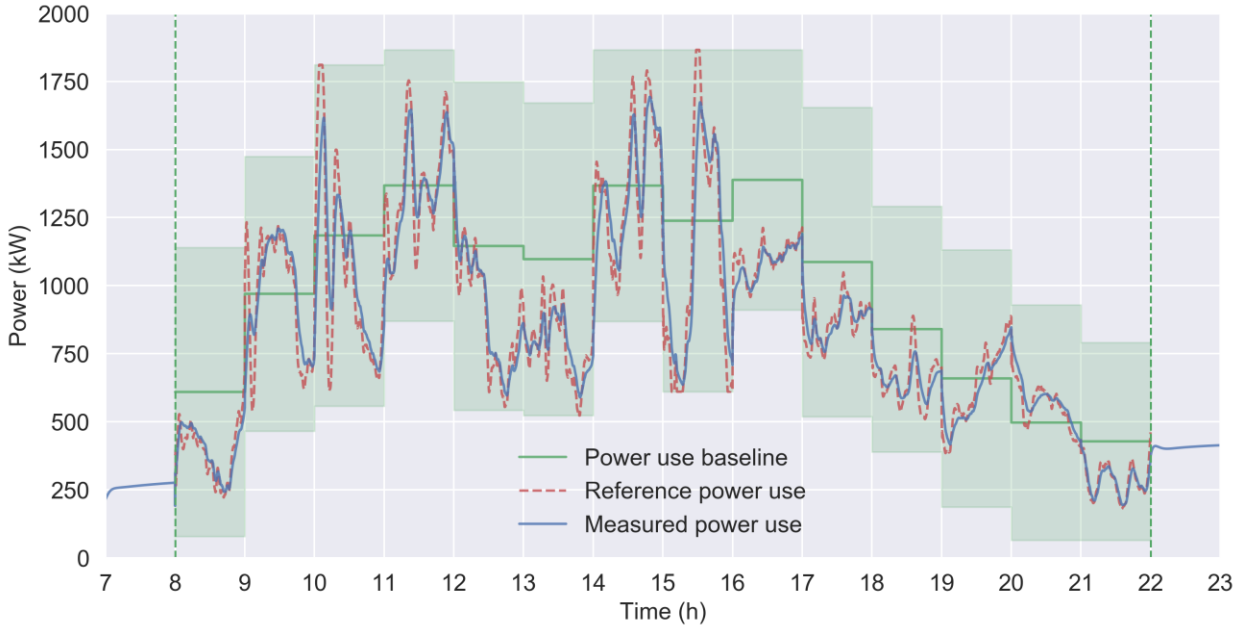

Fig. 14. Power use baseline, reference power use, and measured power use - Test Case 3.

4.4 Test Case 4: Under the proposed control strategy following signal with relatively large hourly maximum accumulated offsets

In Case 4, a signal with large absolute hourly MAOs is selected (237th day in 2018) and followed by the HVAC system. Fig. 15 shows the P_b and four constraints ($P_{cf,h}$, $P_{cf,l}$, $P_{op,h}$, and $P_{op,l}$) of regulation capacity in each hour. In addition, the power use baseline in Case 3 is also presented for comparison. It can be found that the power use baselines in Case 3 and Case 4 are also different. The reason is the same as that mentioned in Section 4.3.

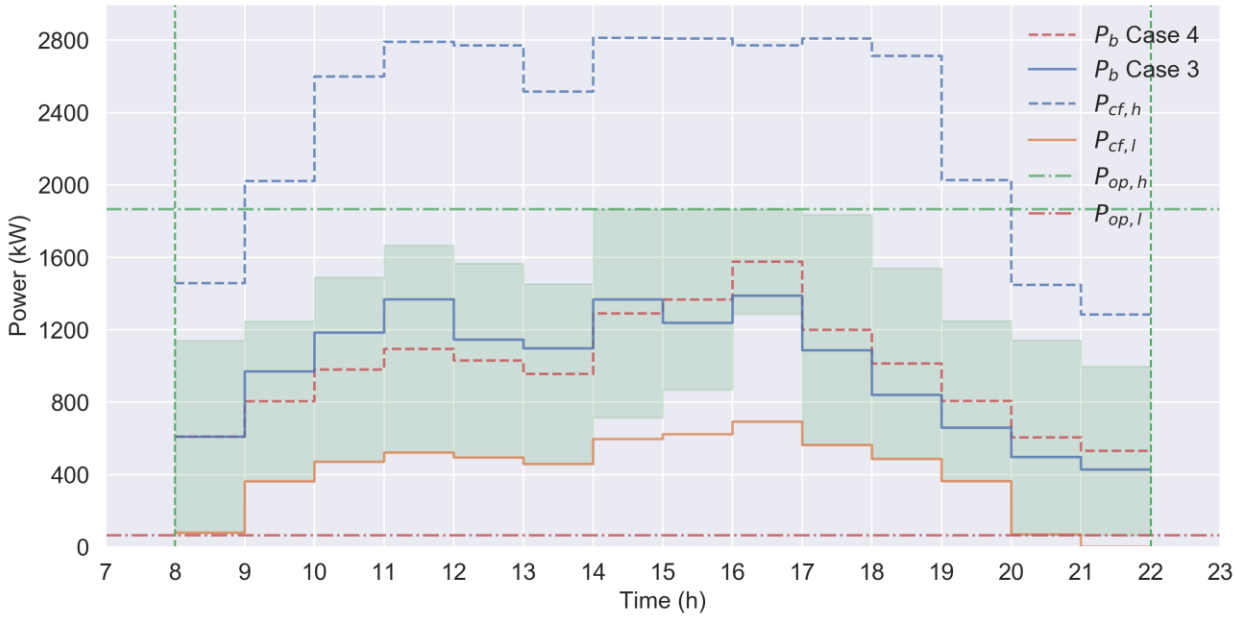

Fig. 15. The power use baseline in Case 3 and the power use baseline and constraints of regulation capacity in Case 4.

Fig. 16 presents the indoor temperature and its setpoint as well as the chilled water supply temperature. Fig. 17 presents the power use baseline, reference power use P_{set}, and measured power use in Case 4. As mentioned in Section 3.3, the guarantee rate (γ) for maintaining the indoor temperature within the comfort range is 0.9. It means under critical conditions when the AGC signal has a large absolute MAO, the indoor temperature may exceed the comfort range. For example, since the measured power use is significantly lower than the power use baseline from 17:00 to 18:00 (shown in Fig. 17), the indoor temperature sometimes exceeded the comfort range during this period (shown in Fig. 16). However, the maximum temperature only exceeded the upper limit of the comfort range slightly in a short time, which could be acceptable in practice. Building managers can also change the guarantee rate after considering the tradeoff between financial reward and thermal comfort. It is worth noticing that around 20:00, the reference power use increased rapidly from its lower limit to its upper limit which was quite challenging for indoor environment control. However, the control strategy still maintained the indoor temperature within the comfort range under such a condition, which further verified the effectiveness of the proposed control strategy.

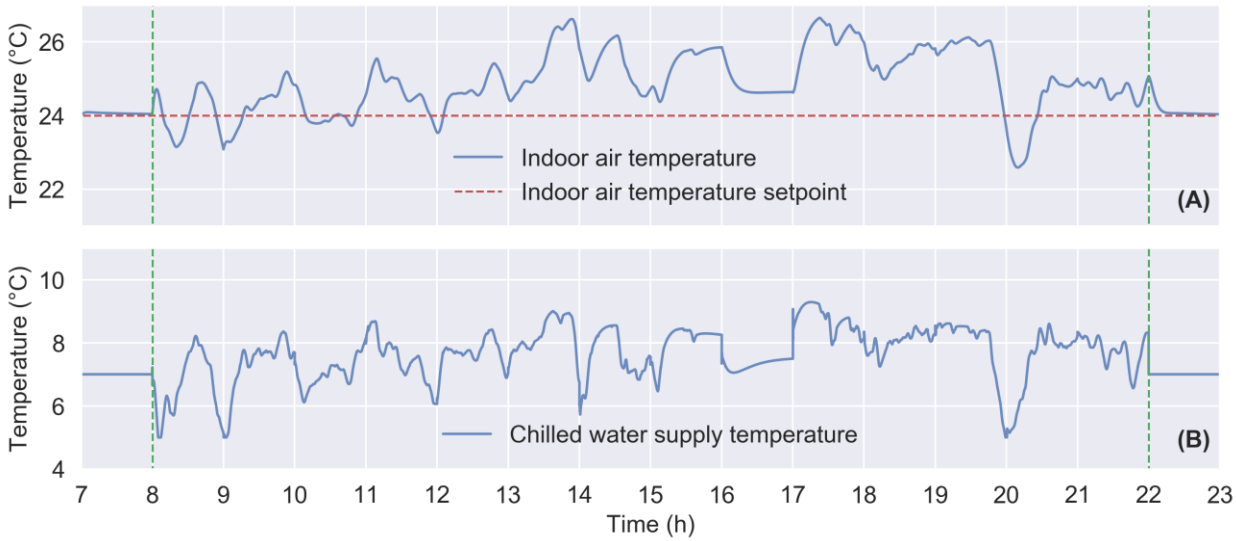

Fig. 16. (A) Indoor temperature and its setpoint (B) chilled water supply temperature - Test Case 4.

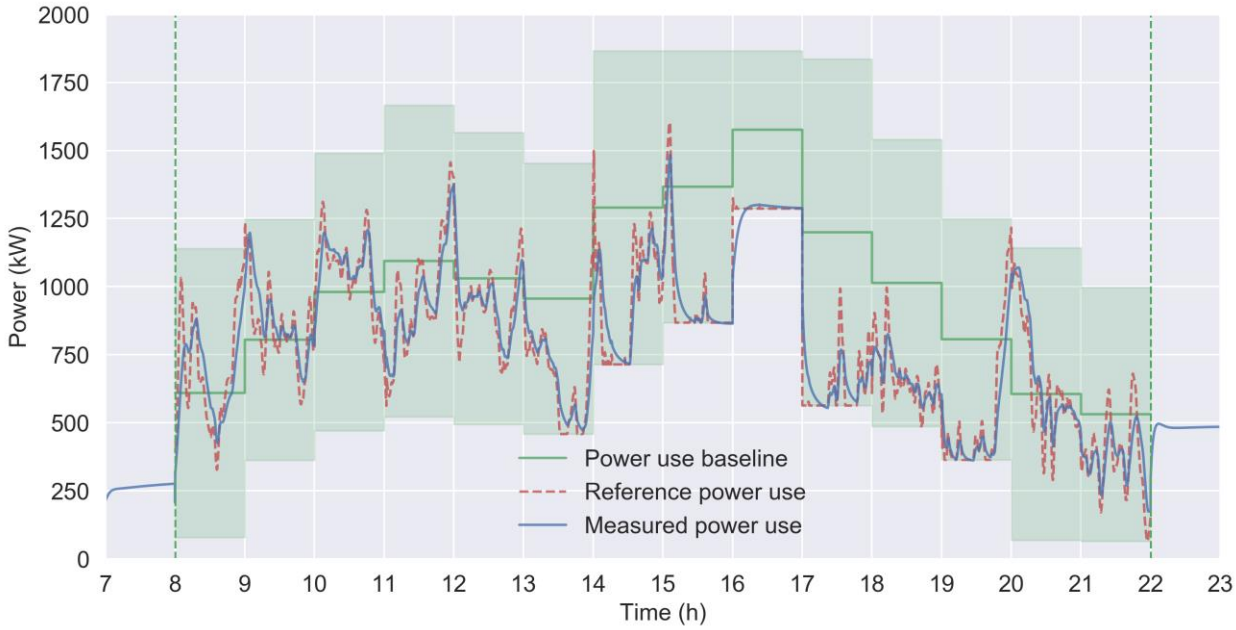

Fig. 17. Power use baseline, reference power use, and measured power - Test Case 4.

5. Discussion and conclusion

In real applications, the systems encountered can be more complicated. For example, many systems have multiple chillers rather than only one chiller, while the control strategy proposed in

this study is also applicable. Of course, more specific new problems can be encountered due to the interactions among different components. These problems will be addressed in our further work.

In a real building, the meter used for measuring the power use of HVAC systems may also be responsible for other consumptions. These consumptions may change all the time although they are non-controllable. When providing frequency regulation service, their measurement should be separated from the HVAC systems. There are two methods, a prediction of these non-controllable consumptions should be firstly considered, which does not need further investment. For another method, a new dedicated meter can be used for the HVAC systems. Of course, this solution needs more investment.

Another problem that needs to be noticed is the control method used by the power use following controller. In this study, it has been emphasized the necessity of simultaneously adjusting the indoor temperature setpoint and chilled water supply temperature setpoint to change the power use of chillers. This paper just uses two PID controllers which may not be the best way. A better control method is worth exploring in the future.

In summary, in this study, a hierarchical optimal control strategy for HVAC systems is proposed to provide frequency regulation service to power grids. This strategy consists of a regulation bidding controller and a power use following controller. Control tests are conducted on a TRNSYS-MATLAB co-simulation platform to test and validate the proposed control strategy. The main conclusions are as follows:

- The hourly “maximum accumulated offset” (MAO) of the frequency regulation signal corresponds to the “maximum temperature offset” (MTO) of the indoor space.
- Although the AGC signal is unpredictable, the hourly MAO of the AGC signal conforms to a stable probability distribution.
- The regulation bidding controller can optimize the power use baseline and regulation capacity, considering the tradeoff between financial reward and thermal comfort while satisfying the operating constraints of HVAC systems.
- The power use following controller can guarantee the response speed and response amount of power use of the HVAC system by modulating the chilled water supply temperature setpoint and the indoor temperature setpoint simultaneously, which can ensure the quality of frequency regulation service.

This study effectively addresses the control of HVAC systems for providing frequency regulation service to power grids. In real applications, the bidding result (i.e., power use baseline and regulation capacity) should be sent to power grids in time. The proposed control strategy does not involve complex optimization technologies, which is very convenient and valuable in actual use. On the other hand, the proposed control strategy also has some limitations. The first one is the simplified building model. This model considers the indoor temperature as a whole, therefore it cannot reflect the temperatures of individual rooms. Another limitation is that the performance of the proposed control strategy depends on the accuracy of the model. Therefore, its performance can be affected if a model with low prediction accuracy is used.

Acknowledgements

The research presented in this paper is financially supported by a research grant under strategic focus area (SFA) scheme of the research institute of sustainable urban development (RISUD) in The Hong Kong Polytechnic University, a general research grant (152165/20E) of the Research Grant Council (RGC) of the Hong Kong SAR. We thank one anonymous reviewer whose comments/suggestions helped improve and clarify this manuscript.

Appendix A. Development of the building thermodynamic model

As shown in Fig. A.1, this model consists of an outdoor side, an envelope, and an indoor side with internal mass. The energy balance is expressed by Eqs. (A.1)-(A.7).

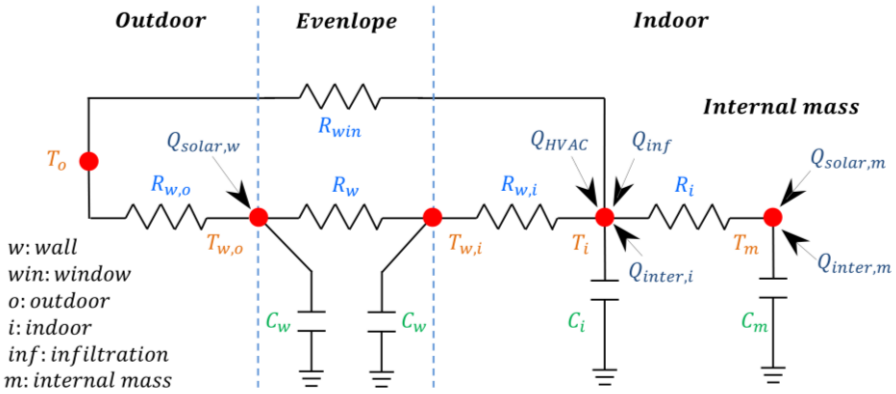

Fig. A.1. Schematic of the building thermodynamic model.

$$C_w \frac{dT_{w,o}}{dt} = \frac{T_0 - T_{w,o}}{R_{w,o}} + \frac{T_{w,i} - T_{w,o}}{R_w} + Q_{solar,w} \tag{A.1}$$

$$C_w \frac{dT_{w,i}}{dt} = \frac{T_{w,o} - T_{w,i}}{R_w} + \frac{T_i - T_{w,i}}{R_{w,i}} \tag{A.2}$$

$$C_i \frac{dT_i}{dt} = \frac{T_{w,i} - T_i}{R_{w,i}} + \frac{T_m - T_i}{R_i} + \frac{T_o - T_i}{R_{win}} + Q_{inter,i} + Q_{HVAC} + Q_{inf} \tag{A.3}$$

$$C_m \frac{dT_m}{dt} = \frac{T_i - T_m}{R_i} + Q_{solar,m} + Q_{inter,m} \tag{A.4}$$

$$Q_{solar,w} = f_{solar,w} A_w I_{solar} \tag{A.5}$$

$$Q_{solar,m} = f_{solar,m} A_{win} I_{solar} \tag{A.6}$$

$$Q_{inf} = \frac{\alpha \cdot (T_o - T_i) \cdot V \cdot C_{air}}{3600} \tag{A.7}$$

R and C represent the overall heat resistance and capacitance; T denotes temperature; Q represents load. Q_{solar} denotes the heat gains from solar radiation, which include the effect on external wall surface ($Q_{solar,w}$) and internal thermal mass ($Q_{solar,m}$). Q_{inter} denotes internal heat gains, which consist of the heat to indoor air ($Q_{inter,i}$), and the heat to internal thermal mass ($Q_{inter,m}$); f denotes the conversion coefficient for heat gains; A denotes geometric area; I_{solar} is global solar radiation; α is air change rate (time per hour). V is the volume of indoor space and C_{air} is the specific heat capacity of air.

The building thermodynamic model described by the ordinary differential Eqs. (A.1)-(A.7) is actually a multiple-input and multiple-output (MIMO) system. This type of system is normally described in the form of state space models due to their advantage in explicitly expressing the relationship between the system outputs and inputs. In addition, state space models can be used to formulate convex optimization problems which in general can be conveniently solved by optimization techniques. Therefore, the building thermodynamic model is switched in the form of a state space model and set up in the MATLAB, as shown in Eq. (A.8).

$$dx/dt = ax + bu + ed \tag{A.8}$$

where the system matrix $a = \begin{pmatrix} \frac{-1}{C_w R_{w,o}} + \frac{-1}{C_w R_w} & \frac{1}{C_w R_w} & 0 & 0 \\ \frac{1}{C_w R_w} & \frac{-1}{C_w R_w} + \frac{-1}{C_w R_{w,i}} & \frac{1}{C_w R_{w,i}} & 0 \\ 0 & \frac{1}{C_i R_{w,i}} & \frac{-1}{C_i R_{w,i}} + \frac{-1}{C_i R_i} + \frac{-1}{C_i R_{win}} - \frac{\alpha V C_{air}}{3600 C_i} & \frac{1}{C_i R_i} \\ 0 & 0 & \frac{1}{C_m R_i} & \frac{-1}{C_m R_i} \end{pmatrix}$, the state vector $x = (T_{w,o} \quad T_{w,i} \quad T_i \quad T_m)^T$. Input matrix $b = (0 \quad 0 \quad 1/C_i \quad 0)^T$. The control input vector matrix $u = (Q_{HVAC})$. The disturbance vector $d = (T_o \quad I_{solar} \quad Q_{inter,i} \quad Q_{inter,m})^T$ .The disturbance matrix $e = \begin{pmatrix} \frac{1}{C_w R_{w,o}} & \frac{f_{solar,w} A_w}{C_w} & 0 & 0 \\ 0 & 0 & 0 & 0 \\ \frac{1}{C_i R_{win}} - \frac{\alpha V C_{air}}{3600 C_i} & 0 & \frac{1}{C_i} & 0 \\ 0 & \frac{f_{solar,m} A_{win}}{C_m} & 0 & \frac{1}{C_m} \end{pmatrix}$.

Appendix B. Validation of the building thermodynamic model

The parameters of the building thermodynamic model are identified by the genetic algorithm optimization technique [37]. The objective of the optimization is to minimize the integrated root mean square error between predicted cooling load and measured cooling load. A five-day (20–25 May) period in a typical year is used for model training. Then, another five-day (26–30 May) period is used for validation. The time step of the prediction is 3 minutes. The comparison between the predicted cooling load and measured cooling load is shown in Fig. B.1.

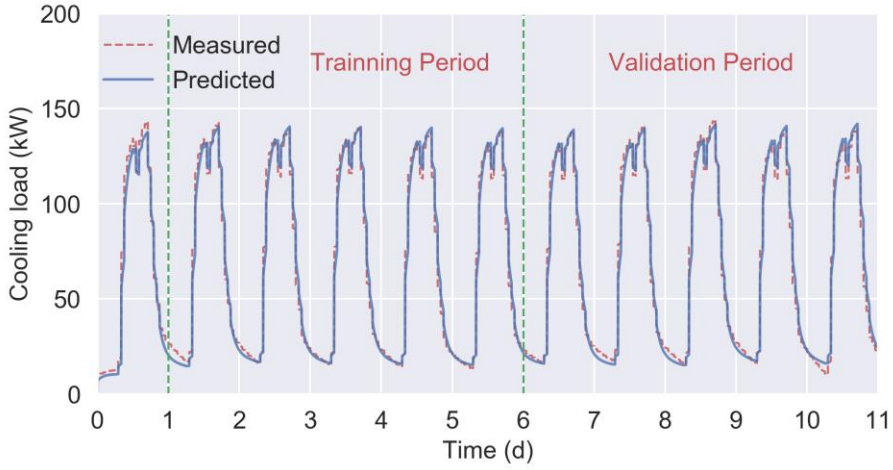

Fig. B.1. Predicted and measured cooling load of the building.

The identification results of the parameters in the building thermodynamic model are listed in Table B1. In order to quantify the prediction performance of the model, three indices are used including the mean absolute error (MAE), mean absolute percentage error (MAPE) and root mean square error (RMSE). The results are listed in Table B2. It can be observed that the building thermodynamic model has a good prediction performance.

Table B.1. Parameters of the building thermodynamic model.

C_m (J/k)	C_i (J/k)	C_w (J/k)	R_i (K/W)
2.70E+08	7.26E+06	2.50E+07	2.50E-05
$R_{w,i}$ (K/W)	$R_{w,o}$ (K/W)	R_w (K/W)	R_{win} (K/W)
2.85E-03	9.98E-04	8.97E-03	7.16E-03

Table B.2. Performance indices of the building thermodynamic model.

	MAE (W)	MAPE (%)	RMSE (W)
Cooling load	3397.08	7.46	4635.64

Appendix C. Dynamic model of the chiller

The power use of a chiller under steady state conditions can be calculated by Eqs. (C.1)-(C.5). Q_{load} is the cooling load of the chiller. m_{chw} represents the flow rate of chilled water. C_{water} is the specific heat capacity of water. $T_{chw,supply}$ and $T_{chw,return}$ are the supply and return chilled water temperature respectively. The part load ratio (PLR) is the ratio of the Q_{load} to the chiller rated capacity ($Q_{HVAC,rated}$). The coefficient of performance (COP) can be obtained from Eqs. (C.3)-(C.4). COP_{rated} is the rated COP and β is relative efficiency to correct the rated COP under different PLRs, which can be obtained from manufacturers [47, 48]. Accordingly, the power use of the chiller at steady state (P_s) can be finally obtained from Eq. (C.5). The transient characteristics of a chiller are extracted from the coupled nonlinear differential equations proposed by He [49], which are based on the mass, momentum, and energy balances of the refrigerant flowing through a heat exchanger tube [50]. According to the experimental study conducted by He [49], in the frequency domain, the change of power use (P) (corresponding to the compressor speed [4]) and $T_{chw,supply}$ can be approximated by the first-order transfer function of the change of the chilled water supply temperature setpoint $\Delta T_{chw,supply,set}(s)$. The transient behavior of the chiller can be then represented by Eqs. (C.6)-(C.7). The power use and $T_{chw,supply}$ in real-time are described by Eqs. (C.8)-(C.9) eventually. The time constant is set as 1 minute. Other coefficients, such as c_1 and c_2, can be obtained according to the steady-state performance of the chiller.

$$Q_{load} = m_{chw} \cdot C_{water} \cdot (T_{chw,return} - T_{chw,supply}) \quad \text{(C.1)}$$

$$PLR = \frac{Q_{load}}{Q_{HVAC,rated}} \quad \text{(C.2)}$$

$$\beta = n_1 \cdot PLR^3 + n_2 \cdot PLR^2 + n_3 \cdot PLR + n_4 \quad \text{(C.3)}$$

$$COP = COP_{rated} \cdot \beta \quad \text{(C.4)}$$

$$P_s = \frac{Q_{load}}{COP} \quad \text{(C.5)}$$

$$\Delta P(s) = \frac{c_1}{s+T} \cdot \Delta T_{chw,supply,set}(s) \quad \text{(C.6)}$$

$$\Delta T_{chw,supply}(s) = \frac{c_2}{s+T} \cdot \Delta T_{chw,supply,set}(s) \quad \text{(C.7)}$$

$$P(t) = P_s + \Delta P(t) \quad \text{(C.8)}$$

$$T_{chw,supply}(t) = T_{chw,supply} + \Delta T_{chw,supply}(t) \quad \text{(C.9)}$$

Reference

[1] Zhao P, Henze GP, Brandemuehl MJ, Cushing VJ, Plamp S. Dynamic frequency regulation resources of commercial buildings through combined building system resources using a supervisory control methodology. Energy and Buildings. 2015;86:137-50.

[2] FERC. Federal Energy Regulatory Commission, FERC Order 755, 2011, https://www.ferc.gov/whats-new/comm-meet/2011/102011/E-28.pdf. 2011. [accessed 16 Feb 2020]

[3] Callaway DS, Hiskens IA. Achieving Controllability of Electric Loads. Proceedings of the IEEE. 2011;99:184-99.

[4] Su L, Norford LK. Demonstration of HVAC chiller control for power grid frequency regulation—Part 1: Controller development and experimental results. Science and Technology for the Built Environment. 2015;21:1134-42.

[5] Su L, Norford LK. Demonstration of HVAC chiller control for power grid frequency regulation—Part 2: Discussion of results and considerations for broader deployment. Science and Technology for the Built Environment. 2015;21:1143-53.

[6] He Hao AK, Yashen Lin, Prabir Barooah, and Sean Meyn. Ancillary service for the grid via control of commercial building HVAC systems. In: American Control Conference; 2013.

[7] PJM Manual 12:Balancing Operations, http://www.pjm.com/~/media/documents/manuals/m12.ashx. [accessed 16 Feb 2020]

[8] Qureshi FA, Jones CN. Hierarchical control of building HVAC system for ancillary services provision. Energy and Buildings. 2018;169:216-27.

[9] Wang H, Wang SW, Tang R. Development of grid-responsive buildings: Opportunities, challenges, capabilities and applications of HVAC systems in non-residential buildings in providing ancillary services by fast demand responses to smart grids. Applied Energy. 2019;250:697-712.

[10] Hong Kong Energy End-use Data 2017, https://www.emsd.gov.hk/filemanager/en/content_762/HKEEUD2017.pdf. [accessed 16 Feb 2020]

[11] Fabietti L, Qureshi FA, Gorecki TT, Salzmann C, Jones CN. Multi-time scale coordination of complementary resources for the provision of ancillary services. Applied Energy. 2018;229:1164-80.

[12] Fabietti L, Gorecki TT, Namor E, Sossan F, Paolone M, Jones CN. Enhancing the dispatchability of distribution networks through utility-scale batteries and flexible demand. Energy and Buildings. 2018;172:125-38.

[13] Cai J, Braun JE. A regulation capacity reset strategy for HVAC frequency regulation control. Energy and Buildings. 2019;185:272-86.

[14] Fabietti L, Gorecki T, Qureshi F, Bitlislioglu A, Lymperopoulos I, Jones C. Experimental Implementation of Frequency Regulation Services Using Commercial Buildings. IEEE Transactions on Smart Grid. 2016:1-.

[15] Lymperopoulos I, Qureshi FA, Nghiem T, Khatir AA, Jones CN. Providing ancillary service with commercial buildings: The Swiss perspective. IFAC-PapersOnLine. 2015;48:6-13.

[16] Gorecki TT, Fabietti L, Qureshi FA, Jones CN. Experimental demonstration of buildings providing frequency regulation services in the Swiss market. Energy and Buildings. 2017;144:229-40.

[17] Vrettos E, Kara EC, MacDonald J, Andersson G, Callaway DS. Experimental Demonstration of Frequency Regulation by Commercial Buildings – Part I: Modeling and Hierarchical Control Design. IEEE Transactions on Smart Grid. 2018;9:3213-23.

[18] Vrettos E, Kara EC, MacDonald J, Andersson G, Callaway DS. Experimental Demonstration of Frequency Regulation by Commercial Buildings – Part II: Results and Performance Evaluation. IEEE Transactions on Smart Grid. 2018;9:3224-34.

[19] Cai J, Braun JE. Laboratory-based assessment of HVAC equipment for power grid frequency regulation: Methods, regulation performance, economics, indoor comfort and energy efficiency. Energy and Buildings. 2019;185:148-61.
[20] Yin R, Kara EC, Li Y, DeForest N, Wang K, Yong T, et al. Quantifying flexibility of commercial and residential loads for demand response using setpoint changes. Applied Energy. 2016;177:149-64.
[21] Wang H, Xu P, Lu X, Yuan D. Methodology of comprehensive building energy performance diagnosis for large commercial buildings at multiple levels. Applied Energy. 2016;169:14-27.
[22] Wang J, Huang S, Wu D, Lu N. Operating a Commercial Building HVAC Load as a Virtual Battery through Airflow Control. IEEE Transactions on Sustainable Energy. 2020:1.
[23] Huang W, Lam H. Using genetic algorithms to optimize controller parameters for HVAC systems. Energy and Buildings. 1997;26:277-82.
[24] Wang SW, Xu X. Simplified building model for transient thermal performance estimation using GA-based parameter identification. International Journal of Thermal Sciences. 2006;45:419-32.
[25] Huang P, Fan C, Zhang X, Wang J. A hierarchical coordinated demand response control for buildings with improved performances at building group. Applied Energy. 2019;242:684-94.
[26] Simon D. Optimal state estimation: Kalman, H infinity, and nonlinear approaches: John Wiley & Sons; 2006.
[27] Daikin_Application Guide Centrifugal Chiller Fundamentals http://www.daikinapplied.com/o365/GetDocument/Doc100/Daikin_AG_31-002_Centrifugal_Chiller_Fundamentals_Guide_Vers_2.2.pdf/. [accessed 16 Feb 2020]
[28] Stasyshan R. Understanding Centrifugal Compressor Capacity Controls. 2015.
[29] Engineering Guide YORK® YZ Centrifugal Chiller www.york.com/-/media/york/next/pdf/york_yz_engineering_guide.pdf. [accessed 16 Feb 2020]
[30] Wang H, Wang SW. The impact of providing frequency regulation service to power grids on indoor environment control and dedicated test signals for buildings. Building and Environment. 2020;183:107217.
[31] Cui C, Zhang X, Cai W, Jing G. A gradient-based adaptive balancing method for dedicated outdoor air system. Building and Environment. 2019;151:15-29.
[32] Cheng Y, Zhang S, Huan C, Oladokun MO, Lin Z. Optimization on fresh outdoor air ratio of air conditioning system with stratum ventilation for both targeted indoor air quality and maximal energy saving. Building and Environment. 2019;147:11-22.
[33] Wang SW, Gao DC, Sun Y, Xiao F. An online adaptive optimal control strategy for complex building chilled water systems involving intermediate heat exchangers. Applied Thermal Engineering. 2013;50:614-28.
[34] Philip C, Chow W. Energy use in commercial buildings in Hong Kong. Applied Energy. 2001;69:243-55.
[35] Hu M, Xiao F, Wang L. Investigation of demand response potentials of residential air conditioners in smart grids using grey-box room thermal model. Applied Energy. 2017;207:324-35.
[36] Johra H, Heiselberg P. Influence of internal thermal mass on the indoor thermal dynamics and integration of phase change materials in furniture for building energy storage: A review. Renewable and Sustainable Energy Reviews. 2017;69:19-32.
[37] Wang SW, Xu X. Parameter estimation of internal thermal mass of building dynamic models using genetic algorithm. Energy Conversion and Management. 2006;47:1927-41.
[38] Li W, Xu P, Lu X, Wang H, Pang Z. Electricity demand response in China: Status, feasible market schemes and pilots. Energy. 2016;114:981-94.
[39] Faria P, Vale Z. Demand response in electrical energy supply: An optimal real time pricing approach. Energy. 2011;36:5374-84.
[40] Chen Y, Chen Z, Xu P, Li W, Sha H, Yang Z, et al. Quantification of electricity flexibility in demand response: Office building case study. Energy. 2019;188.

[41] Clark DR, May WB. HVACSIM+ building systems and equipment simulation program-user's guide. National Bureau of Standards, Washington, DC (USA). Building Equipment Div.1985
[42] Zhou X, Braun J. A Simplified Dynamic Model for Chilled-Water Cooling and Dehumidifying Coils—Part 1: Development (RP-1194). HVAC&R Research. 2007;13:785-804.
[43] Zhou X, Braun J. A Simplified Dynamic Model for Chilled-Water Cooling and Dehumidifying Coils—Part 2: Experimental Validation (RP-1194). HVAC&R Research. 2007;13:805-17.
[44] Wang H, Wang SW, Shan K. Experimental study on the dynamics, quality and impacts of using variable-speed pumps in buildings for frequency regulation of smart power grids. Energy. 2020;199:117406.
[45] Zhuang C, Wang SW. Risk-based online robust optimal control of air-conditioning systems for buildings requiring strict humidity control considering measurement uncertainties. Applied Energy. 2020;261.
[46] Barbero M, Corchero C, Canals Casals L, Igualada L, Heredia FJ. Critical evaluation of European balancing markets to enable the participation of Demand Aggregators. Applied Energy. 2020;264.
[47] Kang J, Wang SW, Gang W. Performance of distributed energy systems in buildings in cooling dominated regions and the impacts of energy policies. Applied Thermal Engineering. 2017;127:281-91.
[48] Shan K, Wang SW, Gao DC, Xiao F. Development and validation of an effective and robust chiller sequence control strategy using data-driven models. Automation in Construction. 2016;65:78-85.
[49] He X-D. Dynamic modeling and multivariable control of vapor compression cycles in air conditioning systems: Massachusetts Institute of Technology; 1996.
[50] Kim YJ, Norford LK, Kirtley JL. Modeling and Analysis of a Variable Speed Heat Pump for Frequency Regulation Through Direct Load Control. IEEE Transactions on Power Systems. 2015;30:397-408.